



## A critical review of reactive vapor deposition for conjugated polymer synthesis

Cite this: DOI: 10.1039/c9tc01388a

David Bilger, S. Zohreh Homayounfar  and Trisha L. Andrew \*

Reactive vapor deposition (RVD) is a nascent, single-step processing method for forming electronic polymer films on unconventional substrates and is increasingly important for creating flexible and wearable electronics. RVD can be interpreted as a solvent-free synthetic technique, where multiple reagents converge in the vapor phase to effect a polymerization reaction. Here, we review reactive vapor deposition of conjugated polymers from a synthetic perspective, starting by establishing its roots in inorganic chemical vapor deposition, tracking its evolution over the recent decade, discussing state-of-the-art monomer and polymer scope, and concluding with an examination of shortcomings where increased attention from the synthetic community would yield impactful advances.

Received 13th March 2019,  
Accepted 31st May 2019

DOI: 10.1039/c9tc01388a

rsc.li/materials-c

### Introduction

Research efforts over the past two decades have reinforced the numerous advantages of  $\pi$ -conjugated macromolecules. As a result, large libraries of polymeric semiconductors have been investigated<sup>1–3</sup> and correlations between their chemical structure, processing conditions,<sup>4</sup> condensed phase morphology,<sup>5</sup> and optical/electronic properties<sup>6,7</sup> are well understood. Of particular interest has been the stretchability<sup>8</sup> and low density<sup>9</sup> of conjugated polymers, which have resulted in unmatched control over processing conditions<sup>10</sup> and enabled nontraditional electronic<sup>11</sup>

and optoelectronic<sup>12</sup> device architectures on arbitrary substrates. Despite such advancements, further efforts are needed to simplify reaction methodologies, increase synthetic accessibility, and make use of unconventional substrates for flexible, wearable and/or implantable electronics. In this regard, vapor deposition techniques have shown great promise as of late.

Reactive vapor deposition (RVD) is a nascent, single-step processing method with which to create functional polymer films on unconventional substrates.<sup>13,14</sup> Recent reviews on this topic eloquently and comprehensively cover the engineering advantages,<sup>15–17</sup> device applications,<sup>18</sup> and scalability of this method.<sup>19</sup> Reactive vapor deposition can be interpreted as a solvent-free synthetic technique, where multiple reagents converge in the vapor phase to effect a polymerization reaction.

Department of Chemistry, University of Massachusetts Amherst, Amherst, MA 01003, USA. E-mail: tandrew@umass.edu



David Bilger

David Bilger is a PhD candidate working under the direction of Professor Andrew in the Department of Chemistry at the University of Massachusetts Amherst. He is currently developing novel monomers and new vapor phase chemistries for synthesizing conjugated polymers using reactive vapor deposition. He received his MS in Polymer and Coatings Science from the California Polytechnic State University in San Luis Obispo while investigating

the surfactant induced self-assembly of liquid crystalline conjugated polymers. He also received his BS in Chemistry from the California Polytechnic State University in San Luis Obispo.



S. Zohreh Homayounfar

S. Zohreh Homayounfar is currently pursuing her PhD in Chemistry under the supervision of Professor Trisha L. Andrew in the Wearable Electronics lab at the University of Massachusetts Amherst. She received her BS and MS in Materials Science and Engineering from Sharif University of Technology (SUT), Tehran, Iran. She designs and creates smart garments embedded with an optimal combination of fabric-based sensors (biopotential, triboelectric, piezo-

electric, strain, and resistive) to monitor human activity and health status.

Here, we review reactive vapor deposition of conjugated polymers from a synthetic perspective, starting by establishing its roots in inorganic chemical vapor deposition, tracking its evolution over the recent decade, discussing state-of-the-art monomer and polymer scope, and concluding with an examination of weak points where increased attention from the synthetic community would yield impactful advances.

## Origins

To thoroughly understand the apparatus and protocols currently used to vapor deposit conjugated polymers, one must start by cogitating on their origins, which lie in the area of inorganic chemical vapor deposition (CVD). CVD is an umbrella term for a suite of deposition methods used to produce complex semiconductor crystals and multilayer structures *via* a chemical reaction (not physical deposition) that takes place from the gas phase at moderate pressures (10 to 760 Torr). All CVD processes boast two unique advantages: (a) exquisite, real time control over the thickness and nanostructure of growing films, and (b) conformal film formation on nonplanar and/or patterned substrates. Due to these unmatched qualities, at least one CVD step is currently integral for the largescale manufacture of microelectronics and optoelectronics. In this section, we highlight three CVD methods that, we believe, act as clear precedents or inspirations for vapor deposition of conjugated polymers: metal–organic chemical vapor deposition (MOCVD), plasma-enhanced chemical vapor deposition (PECVD) and atomic layer deposition (ALD).

MOCVD affords growth of polycrystalline or amorphous semiconductors and thermodynamically-metastable alloys *via* pyrolysis of corresponding organometallic precursors. Desired precursors are volatilized by heating under reduced pressure and transported by inert carrier gases (helium, argon or nitrogen) into a cold-wall reactor equipped with a heated substrate stage (Fig. 1a). Bond cleavage occurs when the precursor vapors

encounter the heated stage, creating reactive species that subsequently couple to form the desired semiconductor or alloy directly on the substrate surface. Representative MOCVD reactions are shown in Fig. 1b and typically involve one organometallic compound and a hydride. The crucial development of MOCVD by Ruhrwein<sup>20</sup> in 1968 allowed growth of III–V and II–VI semiconductors,<sup>21,22</sup> which are still actively used in high performance optoelectronic devices. MOCVD is a medium deposition rate method, whose reaction simplicity allowed for straightforward manufacturability and wide-spread applications in the photovoltaics and semiconductor industries.<sup>23</sup>

At its genesis, the reaction chamber used to perform MOCVD was simply comprised of a thick-walled metal tube, a gas mixture manifold, and a heat source.<sup>24</sup> The metal tube was either oriented such that the gas mixtures would flow horizontally or vertically through the central tube. In the horizontal design, a gradient of film growth was observed across the substrate due to reactant depletion. To address this issue, the substrate holder was placed at an angle of 10° with respect to the incoming gas flux to obtain films of increased uniformity upon depletion of the precursor stream. In the vertical design (named a high-speed rotating disk reactor), the substrate holder was rotated rapidly to pull the precursor vapors to the surface, which averaged out substrate heating disparities and lead to film uniformity over the entire substrate. Once the merits and process details of MOCVD were well established and the technique transitioned into high-throughput production, the standard MOCVD reactor shifted to a “pancake” style (Fig. 1a), which fulfilled the design criteria necessitated by the silicon industry, to selectively augment the effective interaction area between the precursor vapors and the heated substrate, instead of the cold reactor walls.<sup>24</sup>

Building on this foundational work, introducing an electrically-generated plasma into the aforementioned pancake reactor affords PECVD of semiconductors and dielectric materials.<sup>25,26</sup> As illustrated in Fig. 1c, two internal parallel-plate electrodes placed inside the pancake reactor allow for application of a direct or alternating current, which electrically excites the argon carrier gas to generate an argon plasma. The top electrode plate is grounded and a substrate (that is also conductive) is placed on the bottom electrode, which is connected to an electrical power source. A tube reactor variant is also known, where the electrical excitation is created by applying a radiofrequency (RF) discharge *via* external coil electrodes.<sup>27</sup> The reactive species needed to effect a chemical reaction are created by the high energy electrons of the plasma and, therefore, PECVD is performed at low deposition temperatures. This distinguishing feature is a notable advance over MOCVD, which requires high substrate temperatures. PECVD is currently the preferred method with which to create Si, SiO<sub>2</sub>, and Si<sub>3</sub>N<sub>4</sub> films (Fig. 1d), making it a workhorse technique in the manufacture of silicon integrated circuits. PECVD is also used to produce vertically free-standing carbon nanostructures (so-called carbon nanotube “forests”)<sup>28</sup> and graphene multilayers.<sup>29</sup>

Whereas MOCVD and PECVD proved to be indispensable for depositing inorganic semiconductors and dielectric materials, controlled growth of metal oxides and multilayer optical coatings,



**Trisha L. Andrew**

*Trisha L. Andrew is an Associate Professor of Chemistry and Chemical Engineering at the University of Massachusetts Amherst. She directs the Wearable Electronics Lab, a multi-disciplinary research team that produces garment-integrated technologies using reactive vapor deposition. Trisha started her career as an Assistant Professor of Chemistry and Electrical Engineering at the University of Wisconsin-Madison, after receiving her PhD from MIT*

*in 2011. She is a David and Lucile Packard Foundation Fellow, a National Academy of Sciences Kavli Fellow, a L'Oréal USA For Women in Science Fellow, and was named as one Forbes' magazine "30 Under 30" Innovators in Energy.*

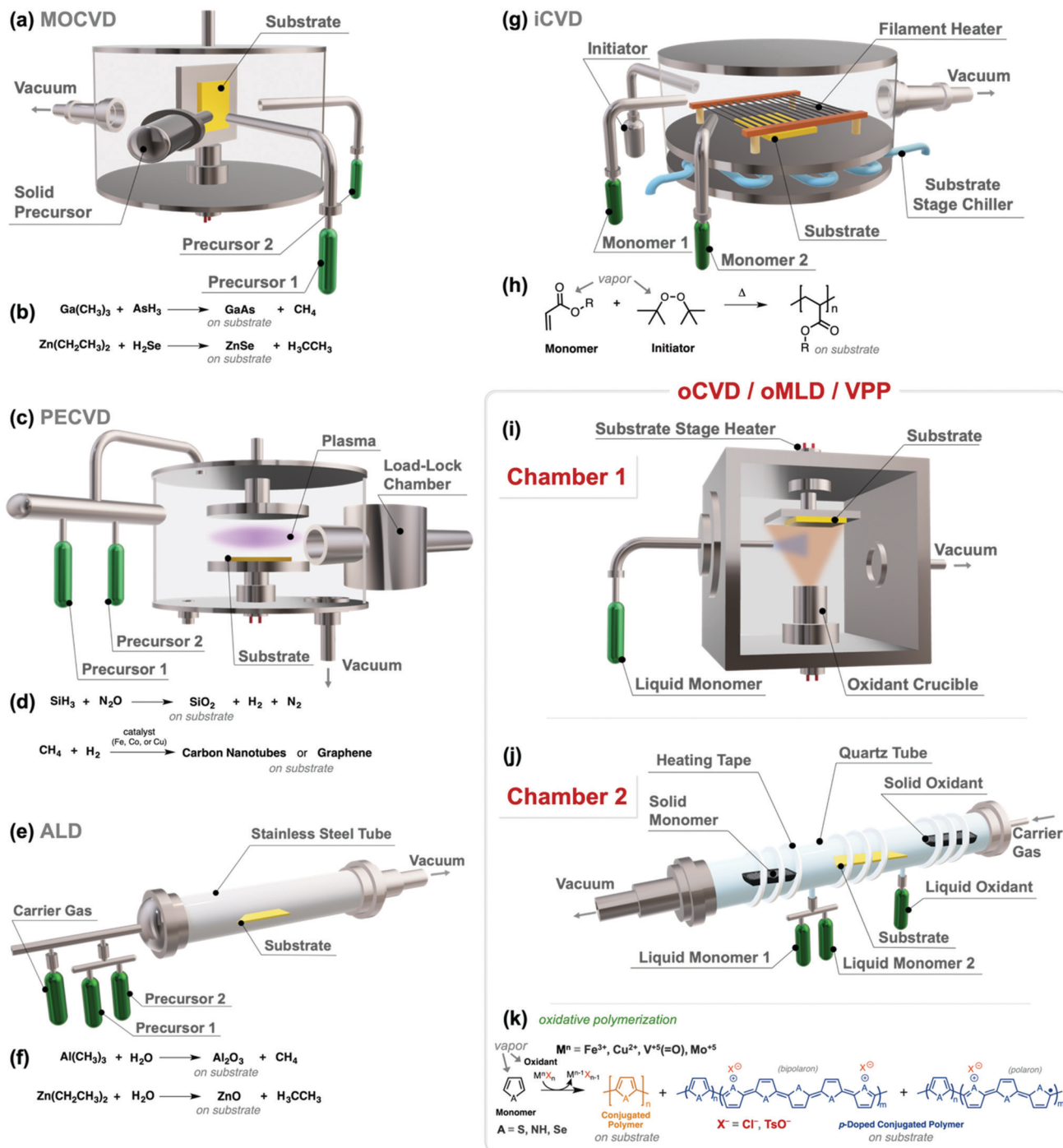


Fig. 1 Schematics of reaction chambers used for common reactive vapor deposition methods. Representative (a) chamber and (b) deposition reactions used in metal–organic chemical vapor deposition (MOCVD). Representative (c) chamber and (d) deposition reactions used in plasma-enhanced chemical vapor deposition (PECVD). Representative (e) chamber and (f) deposition reactions used in atomic layer deposition (ALD). Representative (g) chamber and (h) deposition reaction used in initiated chemical vapor deposition (iCVD). (i and j) Two different chamber geometries for vapor depositing conjugated polymer films. Different deposition algorithms can be used, including oxidative chemical vapor deposition (oCVD), oxidative molecular layer deposition (oMLD) and vapor phase polymerization (VPP). (k) The oxidative polymerization reaction that underpins all known protocols for vapor depositing conjugated polymers.

such as those found in optical fibers and distributed Bragg reflectors, could not be effected using these methods. Therefore, ALD emerged to fill this gap. ALD was first patented by Suntola and Anston<sup>30</sup> in 1977 as atomic layer epitaxy (ALE) for epitaxial

growth of ZnS to produce electroluminescent flat panel displays. The sequential, self-limiting nature of this method led to the growth of thin films which were no longer epitaxial to the underlying substrates. Thus, approximately in 2000, the more general name

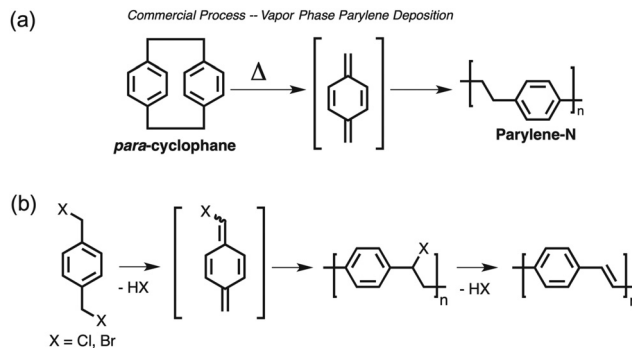
of “ALD” was adopted for this method, recognized as an enabling process in synthesizing nanoscale noble metals (such as Ag, Pd, Os, Ir, Pt), metals (such as C, Al, Fe, Si, Ni, Cu, Ga), metal oxides (such as  $Zn_{1-x}Sn_xO_y$ ,  $ZrO_2$ ,  $Y_2O_3$ ) and optical spacer layers ( $SiO_2$ ,  $Al_2O_3$ ) (Fig. 1f).<sup>31</sup>

In general, ALD is conducted in a stainless-steel horizontal flow tube (Fig. 1e) and involves a repeating algorithm of sequential pulse–purge–pulse cycles. Reactant and counter-reactant precursors are pulsed sequentially into the chamber under vacuum (<1 Torr), reacting one at a time with predetermined active sites on the substrate through a self-limiting reaction mechanism, followed by purging to minimize the possibility of mixing and reacting of precursors in the gas phase. This cycle is iterated until the resulting films reach a desired thickness and composition.<sup>32</sup> ALD’s distinctive pulse–purge–pulse algorithm results in non-statistical film deposition (unlike MOCVD and PECVD), which allows for atomic level control over film composition, thickness and doping level, and creates super-conformal and pinhole-free coatings on high-aspect-ratio nanostructures, such as gate dielectrics in MOSFETs and trench capacitors.<sup>33</sup> However, these advantages come at the expense of deposition speed: in comparison to fast physical vapor deposition methods (such as sputtering and pulsed laser deposition, which typically proceed at a rate of  $5\text{--}10 \text{ \AA s}^{-1}$ ) and medium rate chemical vapor deposition methods (such as MOCVD and PECVD, which typically proceed at a rate of  $1\text{--}2 \text{ \AA s}^{-1}$ ), ALD typically proceeds at a rate of  $0.01 \text{ \AA s}^{-1}$  due to the layer-by-layer growth process and intervening purge cycles. Although attempts to increase deposition rate are ongoing, for example by repeatedly shuttling the substrate between spatially-confined precursor vapor cones,<sup>34,35</sup> ALD still suffers from slow deposition rates that inhibit its widespread use in large-scale manufacturing.

## Emergence

Advances made in the chemical vapor deposition of metal oxides, inorganic semiconductors and dielectric materials eventually piqued the interest of the soft materials community. Specifically, the promise of depositing controllably-thin polymer films conformally onto various patterned and nonplanar surfaces led researchers to modify the aforementioned traditional reactor geometries for vapor-phase organic synthesis. An industrially relevant example of this exercise is the parylene deposition system, which evolved from a two-stage ALD reactor and is now widely used to protect microelectronic circuits from corrosion.<sup>36</sup> Interestingly, this polymeric analog of ALD does not suffer from slow deposition rates, with parylene films grown at an average rate of  $2 \text{ \AA s}^{-1}$ . Similarly, Jensen *et al.* also adapted an ALD reactor to perform a Gilch polymerization reaction from the vapor phase, thus obtaining uniform films of poly(*p*-phenylene vinylene) starting from halogenated *para*-xylylenes (Scheme 1).<sup>37</sup>

An arguably transformative effort in adopting a traditional reactor geometry to effect polymer growth is the reactive vapor deposition of polyacrylate films using a modified MOCVD reactor geometry (Fig. 1g and h), reported by Gleason *et al.*<sup>38</sup>



Scheme 1 (a) Chemical reaction that occurs during parylene deposition. (b) A Gilch polymerization reaction performed from the vapor phase using a modified ALD reactor.

This process, specifically termed initiated chemical vapor deposition (iCVD), allowed for the exquisitely-controlled deposition of various functional polymer films on a myriad of patterned surfaces with varying surface energies.<sup>39</sup> Further, intriguing three-dimensional polymer structures can be created by performing iCVD on liquid<sup>40,41</sup> and/or liquid crystalline surfaces.<sup>42</sup> Previous reviews detail the various advances made in iCVD<sup>43–45</sup> and, therefore, we focus our attention on reactive vapor deposition of conjugated polymers.

Controlled vapor deposition of conjugated polymers is a comparatively exacting endeavor, as small variations in chemical repeat unit structure or compositional defects can exponentially alter the electronic and optical properties of the resulting polymer films. Therefore, reactive vapor deposition of conjugated polymers suffered many false or questionable starts, the most notable of which are reports of poly(thiophene) growth using a glow discharge (PECVD) reactor. Emboldened by the longstanding use of glow discharges to effect undirected chain growth polymerization of hydrocarbon sources for dielectric polymer layers,<sup>46</sup> the PECVD of a material called “plasma polymerized thiophene” was briefly investigated.<sup>47,48</sup> However, it must be remembered that the hot electrons (average energies of 1–5 eV) present in the electrically-generated plasma during PECVD can lead to nonspecific and multiple bond scissions in precursor (thiophene) molecules, which should lead to a statistical mixture of 2- and 3-position linkages between thiophene repeat units and uncontrolled crosslinking between polymer chains. The hot electrons in the plasma can also chemically degrade electron-rich oligomers deposited on the substrate surface, creating species that rapidly react with water and oxygen upon breaking the vacuum of the reactor to form charge traps.<sup>49</sup> Despite selected efforts to pulse the electrically-generated plasma<sup>50</sup> and, thus, mitigate crosslinking and monomer fragmentation, plasma polymerized thiophene was nonetheless riddled with chemical defects that rendered it a comparatively inferior material to solution-synthesized poly(3-alkylthiophene)s.

In an effort to exert a modicum of control over the chemical reaction taking place inside the reactor, materials scientists took a page out of the MOCVD playbook and attempted to conduct straightforward, two-component reactions from the vapor phase to synthesize conjugated polymers. In particular,

the classic oxidative polymerization reaction came to the fore because it simply needed an electron-rich monomer to be mixed with an oxidant (iodine, ferric chloride or nitrosonium tetrafluoroborate) to create low-medium molecular-weight polymers (10–40 kDa) of predictable and well-defined chemical composition via a step-growth pathway.<sup>51,52</sup>

The first attempt at introducing a vapor phase component to the oxidative polymerization reaction was a stepwise deposition protocol where a substrate was preloaded with an oxidant and then passively exposed to monomer vapors in a closed setting. This deposition protocol, which is still employed today, is called vapor phase polymerization (VPP). Often, substrates are coated with oxidant solutions and air-dried before being placed under an inverted crystallization dish along with an open container of a volatile liquid monomer, such as pyrrole. When vapors of the volatile monomer passively diffuse to the oxidant-coated substrate surface,

monomer oxidation and, subsequently, polymerization is initiated.<sup>53</sup> While VPP has undergone numerous changes over the years, including oxidant variation,<sup>54,55</sup> vacuum incorporation,<sup>56</sup> and use of additives,<sup>57–59</sup> the sequential nature of the technique has remained consistent. Upscaling VPP has also proved challenging given its solution processing step, which requires compatibility between both solvent and substrates.<sup>60,61</sup> As such, soft materials researchers realized the need to explore scalable, manufacturing-friendly strategies to perform RVD of conjugated polymers.

The first such strategy, to our knowledge, by Mohammadi *et al.* introduced both the monomer and the oxidant as vapors into a pancake reactor and angled the inlets in such a way that these vapors were forced to intersect over a substrate, on which polymerization proceeded.<sup>62</sup> The generalized mechanism for the polymerization that is effected when monomer and oxidant vapors interact is depicted in Fig. 2. Due to their reasonable

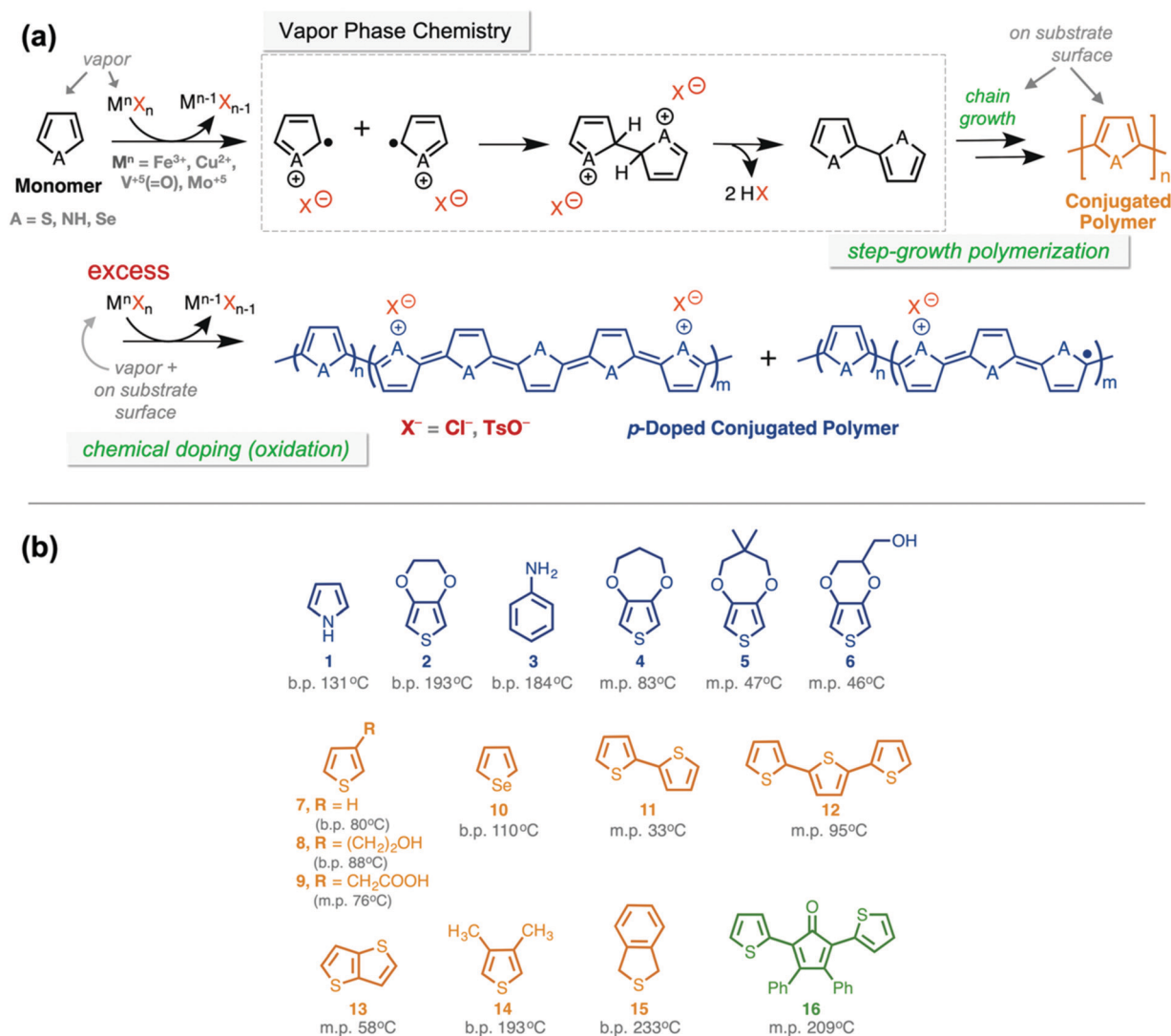


**Fig. 2** (a) Commonly accepted reaction mechanism for reactive vapor deposition of conjugated polymers using an oxidative polymerization reaction. Note that a p-doped film is obtained. (b) A representative set of monomers that have been polymerized via reactive vapor deposition. Polymer films resulting from use of monomers depicted in blue remain p-doped after a post deposition rinse, whereas films resulting from monomers depicted in orange are dedoped after rinsing. Monomer 16, shown in green, creates an electron-accepting polymer.

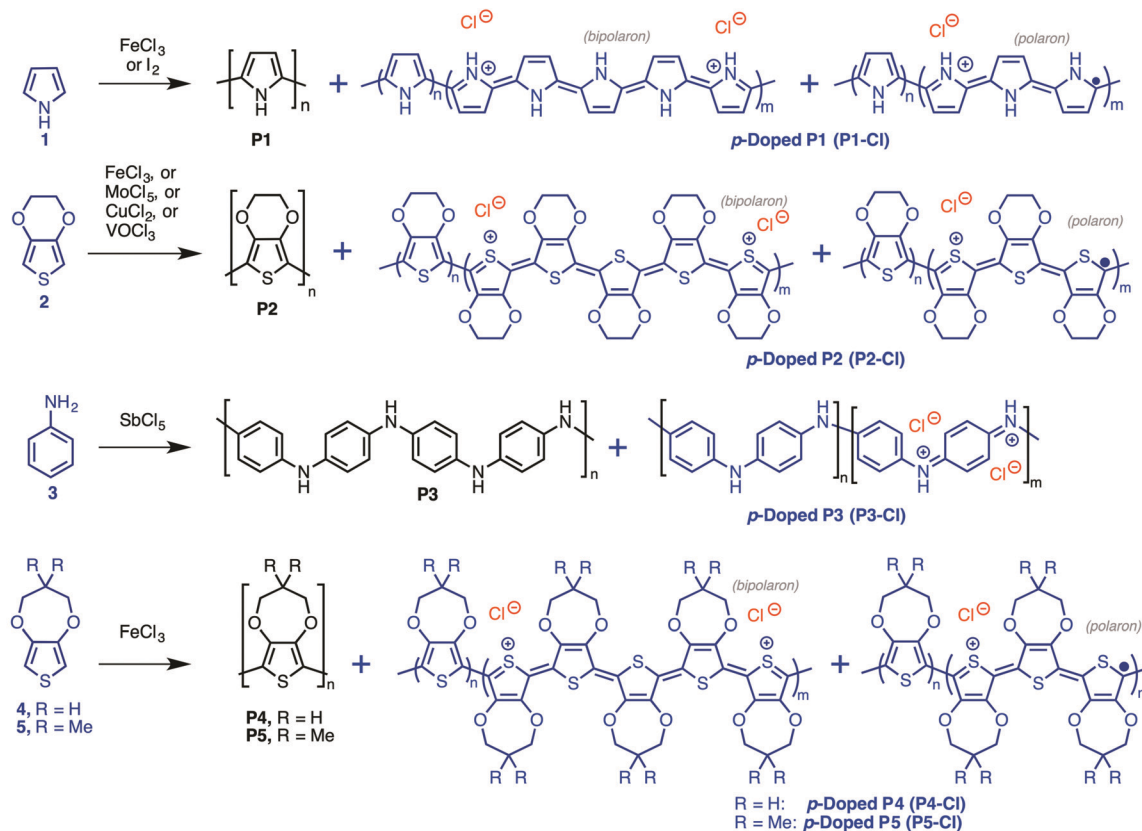
vapor pressures and thermal stabilities, pyrrole (**1**) and iron(III) chloride ( $\text{FeCl}_3$ ) were used as the monomer and oxidant, respectively, to create thin films of p-doped poly(pyrrole) (**P1-Cl**, Scheme 2). Mohammadi *et al.* made certain modifications to the traditional MOCVD reactor inlets to accommodate both precursors. In the case of **1**, a glass tube was articulated with a needle valve *via* a glass-to-metal seal so that the copper tube could be positioned inside the reactor at a distance of 2 cm from the substrate stage.  $\text{FeCl}_3$  was introduced into the reactor *via* a stainless steel tube that was welded in place of a liquid precursor inlet. Mechanistically, simultaneous introduction of monomer and oxidant vapors into the reaction chamber allowed radical cations of monomer **1** to form in high concentration, in the vapor phase, prior to dimerization.<sup>63</sup>

Because dimerized species had significantly lower vapor pressures relative to their corresponding monomers, polymer growth and chain extension likely occurred on the substrate surface.<sup>45</sup> The presence of excess metal salts throughout the deposition further oxidized the polymer film, leaving behind p-doped **P1-Cl**. Subsequent rinsing of the **P1-Cl** films with ethanol removed metal salts, excess oxidant, and any soluble byproducts trapped within the film.

After this successful demonstration of conjugated polymer RVD, subsequent reactors were automatically designed around the two-component oxidative polymerization reaction, which is ideally suited for dry vacuum processing techniques. As can be seen in Fig. 1i–k, a reaction consisting of two components can

be easily performed in any reactor geometry, as only two inlets are required to accommodate the deposition precursors. Further, use of a dry vacuum process eliminates issues associated with solvent considerations, including solvation shells,<sup>64</sup> immiscibility,<sup>65</sup> solvent–substrate interactions,<sup>66</sup> and solubility of the growing polymer chain.<sup>67</sup> Over the past two decades, approximately, a small set of electron-rich monomers have been polymerized *via* reactive vapor deposition (Fig. 2b).

The reactor geometry utilized by Mohammadi *et al.* was only able to create uniform polymer films over areas of approximately 13 cm<sup>2</sup>, which limited its amenability to production-scale applications. To remedy this restriction, Gleason and coworkers designed a reactor capable of yielding uniform polymer films over larger areas (26–52 cm<sup>2</sup>). As illustrated in Fig. 1i, a 168 cm<sup>3</sup> cube-shaped reaction chamber created long monomer and oxidant path lengths (*ca.* 17 cm), analogous to the chambers used for physical vapor deposition of molecular semiconductors in organic light-emitting diodes.<sup>68,69</sup> This is in direct opposition to the chamber dimensions of Mohammadi *et al.*, in which the monomer and oxidant inlets were positioned approximately 2 cm from the substrate stage. Longer path lengths allow for greater stabilization and equilibration of the kinetic energies and trajectories of gas-phase species, thereby increasing the uniformity and conformality of films formed when precursor vapors intersect.<sup>70</sup> The first chamber reported by Gleason *et al.* placed the oxidant crucible, inverted, over the substrate stage, but such an arrangement



Scheme 2 Reactive vapor deposition of conducting polymers.

resulted in the transfer of oxidant particulates to the film surface during deposition.<sup>45</sup> The flipped geometry was then identified to be optimal, with the inverted substrate stage placed above the oxidant crucible and monomer inlet(s) placed perpendicular to the oxidant plume (Fig. 1i, Chamber 1). Monomer and oxidant vapor plumes intersect at a 90° angle, thereby increasing their total intersectional volume (reaction zone) and creating a large, homogenous area (>26 cm<sup>2</sup>) over which dimers, oligomers and polymers are created.

Graduates from Gleason's lab have since made small modifications to this starting design. For example, juxtaposing two crucibles in parallel at the base of the chamber allows for volatilization of heavy, high melting point monomers, such as porphyrin derivatives (molecular weights >400 g mol<sup>-1</sup>, melting points >350 °C), alongside a ferric chloride oxidant.<sup>71,72</sup> However, the intersectional area between monomer and oxidant vapor plumes in this reactor is smaller, as compared to Gleason's original design, meaning that only small-area polymer films can be accessed. Moreover, monomers of intermediate molecular weight and vapor pressures—for example, a solid monomer with a molecular mass of 150 g mol<sup>-1</sup> and melting point of 80 °C—cannot be controllably volatilized in a heated crucible, which is best suited for compounds of melting points >300 °C.

A different approach from that reported by Gleason *et al.* is to adopt a design similar to the tube-shaped reactors used for ALD. Indeed, horizontally-oriented tube reactors have previously been used to deposit dielectric<sup>73</sup> and metal-organic hybrid polymers<sup>31</sup> using a technique commonly referred to as molecular layer deposition (MLD). This geometry has since been adapted by Andrew *et al.* to deposit conjugated polymers *via* reactive vapor deposition. As depicted in Fig. 1j, the geometry of a tube-shaped hot-wall reactor (Chamber 2) provides short and linear paths for monomer and oxidant vapors to traverse, meaning that monomers and oxidants with either high or low vapor pressures can be controllably volatilized with minimal heating and that their vapors can be practically manipulated to intersect over a defined spatial extent.<sup>74</sup> Side inlets are built into the chamber body to introduce volatile and/or liquid oxidants or monomers into the central reaction tube. Crucibles (tungsten or ceramic) filled with solid monomers or oxidants may also be placed directly in the tube for easy heating/volatilization. Upon selectively heating the specific regions of the tube in which the monomer and/or oxidant are placed, vapors evolve that move parallel to the chamber's long axis and intersect over a substrate region, effecting vapor-phase monomer oxidation/dimerization and chain growth at the substrate surface. The primary advantages of this chamber are its modularity and ability to accommodate a wide range of low-to-high volatility compounds, making it ideal for testing pilot monomers and new vapor phase chemistries.

Over the past decade, Chambers 1 and 2 have been centrally used to conduct various polymer deposition algorithms, with each protocol garnering a specific categorization. For example, a substrate could simply be preloaded with an oxidant, placed in Chamber 1 and exposed to a monomer vapor flow through the side inlet to obtain a conjugated polymer coating on the substrate.<sup>75</sup> Or, monomer and oxidant vapors can be sequentially pulsed into Chamber 2, perhaps with intervening inert gas purges,

similar to ALD/MLD, to create thin, nanostructured polymer films over multiple iterations.<sup>76</sup> For this review, we classify any deposition algorithm in which a substrate is preloaded with oxidant as VPP, any protocol in which monomer and oxidant vapors are simultaneously and continuously introduced into a reaction chamber throughout the deposition as oxidative chemical vapor deposition (oCVD), and any pulsed deposition protocol as oxidative molecular layer deposition (oMLD). We note that the oCVD protocol is, by far, the most common algorithm used across multiple research reports and multiple reactors, and is largely accepted as the default protocol within the field. In situations where we do not wish to invoke a specific deposition protocol, we use the general term “reactive vapor deposition (RVD)” to broadly refer to any process that creates polymer films *via* a chemical reaction that takes place from the vapor phase.

## State of the art

The most extensively investigated precursor, by far, is monomer 2 due to its high vapor pressure, reasonable thermal stability and low oxidation potential.<sup>15,45,63,66,70</sup> Further, monomer 2 has been coupled with a number of oxidants for reactive vapor deposition, including ferric chloride (most common), copper(II) chloride, vanadium oxychloride, molybdenum(V) pentachloride, and molecular bromine. Remarkably high conductivities are observed in vapor deposited thin films of **P2-Cl** (Scheme 2), since resistive, solubilizing counterions are unnecessary for polymer/film growth. Using the oCVD protocol with FeCl<sub>3</sub>, Gleason *et al.* were able to achieve conductivities as high as 6259 S cm<sup>-1</sup> in crystalline PEDOT samples by heating their substrates to 300 °C during deposition and precisely controlling polymer film thickness (10 nm).<sup>77,78</sup> Given these parameters, X-ray diffraction studies elucidated an induced crystalline transition from an “edge on” to “face on” orientation with increasing substrate temperature and decreasing **P2-Cl** film thickness. Such a feat reinforces the capability of reactive vapor deposition protocols and chamber parameters to influence the properties of conjugated polymer thin films.

Parsons *et al.* also experimented with chamber parameters and deposition protocols to access **P2-Cl** films.<sup>76</sup> An oMLD approach was utilized with a molybdenum(V) pentachloride (MoCl<sub>5</sub>) oxidant, chosen due to its comparatively high vapor pressure. As such, low substrate temperatures (<150 °C) could be used during a deposition, making this process compatible with flexible and textile substrates. The sequential pulsing of precursors *via* oMLD resulted in **P2-Cl** conductivities as high as 5300 S cm<sup>-1</sup>. Such high conductivities were postulated to result from the sequential vapor pulsing, which likely increases precursor and byproduct mobility at the substrate surface and allows growing **P2-Cl** chains to adopt an ideal, thermodynamically-stable crystal orientation. Aside from MoCl<sub>5</sub>, other oxidants have been utilized in the reactive vapor deposition of **P2-Cl**, including copper(II) chloride, which results in highly-porous, nanostructured films.<sup>79</sup>

Investigations conducted by Andrew *et al.* have illuminated fundamental differences between the film properties of **P2-Cl**

samples processed using VPP protocols as opposed to oCVD.<sup>75</sup> By way of cyclic voltammetry and electrogravimetry measurements, repeated doping/dedoping cycles demonstrate almost negligible ion mass trapping in **P2-Cl** films coated onto gold electrodes using oCVD. In contrast, films created by a VPP protocol show significant ion mass trapping with each doping/dedoping cycle, suggesting oCVD-produced **P2-Cl** is comparatively more stable to redox cycling. Andrew *et al.* hypothesized that the superior ion transport of oCVD-**P2-Cl** results from its microscopically smooth surface consisting of nano-pores with uniform size, as revealed *via* scanning electron microscopy (SEM). **P2-Cl** constructed using VPP, in contrast, demonstrated rough surfaces with wide distributions of pore sizes, possibly hindering ion transport.

Nejati *et al.* coated commercial carbon cloth with **P2-Cl** films using oCVD and either  $\text{SbCl}_5$  or  $\text{VOCl}_3$  as the oxidant.<sup>80</sup> Conductivities of approximately  $2000 \text{ S cm}^{-1}$  were measured and partly attributed to residual antimony salts remaining in the polymer film. This is one of a few instances where the authors deliberately chose not to perform a post-deposition rinse to wash residual metal salts out of the deposited films. Residual metal salts imparted unique electroactivity and were found to be beneficial for effecting electrochemical oxygen reduction when two **P2-Cl** coated carbon cloths were used as electrodes.

Andrew *et al.* used oCVD polymer films in wearable micro-supercapacitors (MSCs).<sup>81</sup> **P2-Cl** deposited by oCVD was chosen for its demonstrated mechanical ruggedness on multiple fabric substrates.<sup>63</sup> Chamber 1 was used to coat stainless steel threads with **P2-Cl**. The **P2-Cl**-coated threads were sewn into stretchy textiles *via* a four step sequential process, thereby forming aligned electrodes with dimensions dependent on the textiles knit structure. When incorporated with a poly(vinyl alcohol)/sulfuric acid gel electrolyte, the textile MSC displayed an areal capacitance and energy density of  $80 \text{ mF cm}^{-2}$  and  $11 \mu\text{W h cm}^{-2}$ , respectively. After 4000 charge/discharge cycles, the textile MSC retained 71% of its initial capacitance, which recovered to 93% given a 12 hour resting period. This result was highly reproducible and speculated to originate from unbalanced charges redistributing throughout the device. In addition, the textile MSCs energy density could be increased to  $34 \mu\text{W h cm}^{-2}$  when fabricated with a 1-ethyl-3-methylimidazolium tetrafluoroborate ionic liquid electrolyte.

Further studies regarding **P2-Cl**-based charge storage devices were also conducted. By depositing **P2-Cl** onto different varieties of plant matter using oCVD,<sup>82</sup> the **P2-Cl** coating was able to conformally adopt the mesoscale organization of the plant surfaces, with the living substrates remaining undamaged. Pseudocapacitive properties (areal capacitance, energy density, and power density) of the **P2-Cl**-coated plant matter were then measured using two-electrode cyclic voltammetry, with an aqueous sulfuric acid liquid electrolyte, and compared to those of control **P2-Cl** films on polyimide substrates. **P2-Cl** coated onto *Pilea involucrata* showed the greatest discrepancy in pseudocapacitive behavior relative to control samples on polyimide, with an areal capacitance, energy density, and power density of  $142 \text{ mF cm}^{-2}$ ,  $28.4 \mu\text{W h cm}^{-2}$ , and  $1.7 \text{ mW cm}^{-2}$ , respectively. This is in contrast to **P2-Cl** deposited onto polyimide, which displayed lower values

of  $50 \text{ mF cm}^{-2}$ ,  $10 \mu\text{W h cm}^{-2}$ , and  $0.6 \text{ mW cm}^{-2}$  for areal capacitance, energy density, and power density, respectively. Moreover, after 10 000 charge–discharge cycles, **P2-Cl**-coated plant substrates exhibit 94% of their initial capacitance, suggesting the electrodes are remarkably stable.

Aside from Andrew *et al.*, Lau and coworkers frequently use reactive vapor deposited poly(aniline)s for charge storage applications. Vapor deposition is performed using an oCVD protocol with antimony(v) pentachloride and 3 as oxidant and monomer, respectively, to afford **P3-Cl**.<sup>83</sup> Lau *et al.* used an oCVD protocol to systematically deposit numerous samples of **P3-Cl** onto molybdenum carbide-derived-carbon (CDC) electrodes by varying deposition parameters, including reactor pressure, substrate temperature, and oxidant flow rate. The **P3-Cl**-coated CDC electrodes were incorporated into a standard three-electrode configuration consisting of an overcapacitive activated carbon counter-electrode and a  $\text{Ag/AgCl}$  reference electrode in KCl. Electrochemical measurements showed **P3-Cl**-coated CDC electrodes possessed a gravimetric capacitance of  $115 \text{ F g}^{-1}$ , more than double that of control CDC electrodes at  $52 \text{ F g}^{-1}$ . After running over 10 000 charge–discharge cycles, the **P3-Cl**-coated electrodes retained 79% of their initial capacity. Importantly, the highest performing **P3-Cl**-coated electrodes were produced using the highest reactor pressure, substrate temperature, and oxidant flow rate. Scanning electron micrographs (SEMs) of the optimized samples showed significant porosity over films created using alternative deposition protocols. The authors surmised that superior electrochemical properties likely arose due to the presence of pores in the **P3-Cl** films, which provides more surface area for charge accumulation at the electrode–electrolyte interface.

Andrew *et al.* also demonstrated numerous applications in energy conversion and harvesting. Cotton fabrics and yarns coated with **P2-Cl** using Chamber 1 acted as electric heaters that could be cut/sewn or woven to fashion lightweight fabric heaters for local climate control and personal thermal management.<sup>84</sup> Prewoven fabrics coated, *via* oCVD, with a 1.5-micron thick film of **P2-Cl** possessed competitively-low sheet resistances— $44 \Omega \square^{-1}$  measured for coated bast fiber textiles and  $61 \Omega \square^{-1}$  measured for coated cotton textiles—and acted as low-power-consuming Joule heating elements. The electrothermal response of the textile electrodes remained unaffected after cutting and sewing due to the robustness of the vapor deposited coating. This feature was used to create a lightweight, breathable, electrically-heated glove.

More recent studies by Andrew *et al.* have looked into engineering all-fabric wearable thermoelectric generators that produce power over an extended period of time.<sup>85</sup> Using Chamber 2, monomer 2 and  $\text{FeCl}_3$  were reacted to form rectangular coatings of **P2-Cl** on the surface of cotton using a shadow mask. The **P2-Cl**-coated cotton segment was incorporated into a fabric-based wristband that generated thermovoltages above 20 mV when worn. The power factor, measured over a  $30 \text{ }^\circ\text{C}$  temperature differential, of cotton coated with **P2-Cl** *via* oCVD was over two orders of magnitude higher than cotton coated with PEDOT:PSS by solution processing.

Various analogues of **P2-Cl** have also been deposited by Andrew *et al.* using Chamber 2. In one such case, **P4-Cl** (Scheme 2), which is a solid at room temperature, was deposited on the outer surfaces of

plants to act as electrode pads for bioimpedance spectroscopy.<sup>86</sup> **P4-Cl** was chosen for use in this study due to its porous morphology, which aids in measurement accuracy with electronic impedance spectroscopy and was found to not interrupt plant growth. By way of bioimpedance spectroscopy, the **P4-Cl** electrodes were able to monitor plant stressors, including drought and photodamage.

Extensive work has gone into investigating the reactive vapor deposition of semiconducting polymers using oCVD protocols (Scheme 3). Thiophene monomers lacking alkoxy substituents in the 3- and/or 4-position afford light-absorbing, hole-conducting (p-type) polymer films. Gleason *et al.* used Chamber 1 to create ultrathin films of **P7** for use in p-channel organic field-effect transistors.<sup>87</sup> The optoelectronic properties as a function of pressure were examined, with high background chamber pressures producing films of decreased conjugation length compared to films deposited under relatively low chamber pressures. Further, **P7** films fabricated using high chamber pressures demonstrated increased field effect mobility ( $3.74 \times 10^{-3} \text{ cm}^2 \text{ V}^{-1} \text{ s}^{-1}$  at 150 mTorr) compared to low-pressure depositions ( $1.80 \times 10^{-4} \text{ cm}^2 \text{ V}^{-1} \text{ s}^{-1}$  at 1 mTorr). A follow up to this work incorporated vapor deposited **P7** into a bilayer solar cell with physical vapor deposited  $\text{C}_{60}$  as the acceptor layer.<sup>88</sup> Solar cells containing an oCVD deposited **P7** layer demonstrated similar power conversion efficiencies as solution-processed bilayer devices containing poly(3-alkylthiophene)s.

Notably, thiophene-based polymers lacking 3,4-dialkoxy substituents in their repeat unit were dedoped during the post-deposition solvent rinsing step (Fig. 3). Dedoping was evident in UV-vis absorption spectra of **P13** films recorded immediately after deposition and after various rinsing times. In contrast, vapor deposited films of **P3-Cl**, which were created using a 3,4-dialkoxythiophene monomer, remained persistently p-doped, even after solvent rinsing and extended exposure to ambient. X-ray photoelectron spectroscopy and energy dispersive X-ray spectroscopy of **P3-Cl** and **P13** films, respectively, confirmed that metal salts were completely rinsed out of both samples. Therefore, such differing behavior cannot be explained by invoking metal impurities. Instead, the intrinsic ability of each polymer repeat unit structure to stabilize polaronic or bipolaronic charge carriers determines whether a polymer film will be dedoped during rinsing.<sup>89,90</sup>

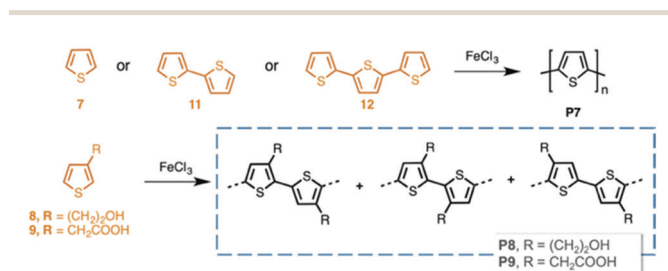
Another point to consider is the nature of the linkages between repeat units in vapor deposited poly(thiophene)s (Scheme 4). Since an oxidative polymerization underpins all known vapor deposition recipes, the reactive species responsible for chain extension is a

thiophene radical cation, which displays notable electron density in both the  $\alpha$ - and  $\beta$ -positions of the thiophene ring. Therefore, intermolecular coupling of these radical cations can produce a statistical mixture of both  $\alpha$ -linkages, and undesirable  $\beta$ -linkages and crosslinks.

Further work done by Gleason *et al.* investigated the use of conjugated polymers with reactive side-chain moieties to allow for post-deposition functionalization. In one study, monomers **2** and **8** were co-deposited using an oCVD protocol.<sup>91</sup> The use of **8** enabled the deposited copolymer to be decorated with hydroxyl groups that proved useful for future work concerning chemiresistive biosensors.<sup>92</sup> The incorporation of hydroxyl groups into the copolymer allowed for immobilization of avidin onto the copolymer surface, which in turn was able to specifically bind biotin (analyte). In a similar approach, carboxylic acid functionalized conducting copolymers were prepared using oCVD through co-evaporation of **2** and **9** with  $\text{FeCl}_3$ .<sup>93</sup> Regulating the ratio of monomers **2** and **9** enabled the authors to control the extent of chemical functionality in the resulting films. Silver nanoparticles were assembled on the surface of the conducting copolymers, suggesting these materials may prove useful for sensor applications. A follow up to this work created copolymer films *via* oCVD for sensing of volatile organic compounds.<sup>94</sup> Compounds **2** and **9** were chosen as comonomers and deposited *via* oCVD. A chemical crosslinker was covalently attached onto the surface of the conductive copolymers and different metals were then assembled onto the unfunctionalized end of the linker molecule. Analyte vapor was then flown over the hybrid conducting copolymer-metal surface. Chemisorption of the analyte led to changes in the metal work function, thereby altering the electronic states of the conducting copolymer film and producing a signal. In addition, **P10** was synthesized using oCVD (Scheme 5) and possessed a band gap of approximately 1.72 eV, which is relatively low compared to many standard thiophene-based polymers.<sup>95</sup>

In an effort to expand the scope of monomers that can be used in reactive vapor deposition, Andrew *et al.* utilized Chamber 2 to deposit various polymers starting from intermediate molecular weight precursors that are solids at room temperature and ambient pressure (Fig. 2).<sup>74</sup> Polymers created using monomers **4**, **5**, **6**, **11**, **12**, and **13** were deposited successfully onto various textured surfaces using Chamber 2. Importantly, no polymer films were observed when the same monomers were loaded into Chamber 1. Andrew *et al.* hypothesized that the precursor path lengths in Chamber 1 were too long and lead to impractically-low mean free paths for reactant vapors. Further characterization of **P13** films confirmed that Chamber 2 was able to uniformly and conformally coat highly-textured surfaces to the same degree as Chamber 1 (Fig. 4). In addition, **P13** displayed excellent adherence to fabric substrates after numerous rubbing and washing cycles, reinforcing that this polymer can be used as effectively as **P2-Cl** in wearable electronics.

Thick films of **P14** grown on flexible polyimide substrates using Chamber 1 were observed to produce large operating voltage windows in two-electrode supercapacitor devices (Fig. 5). As mentioned earlier, thick films of **P2-Cl** served as effective single



Scheme 3 Reactive vapor deposition of semiconducting polymers.

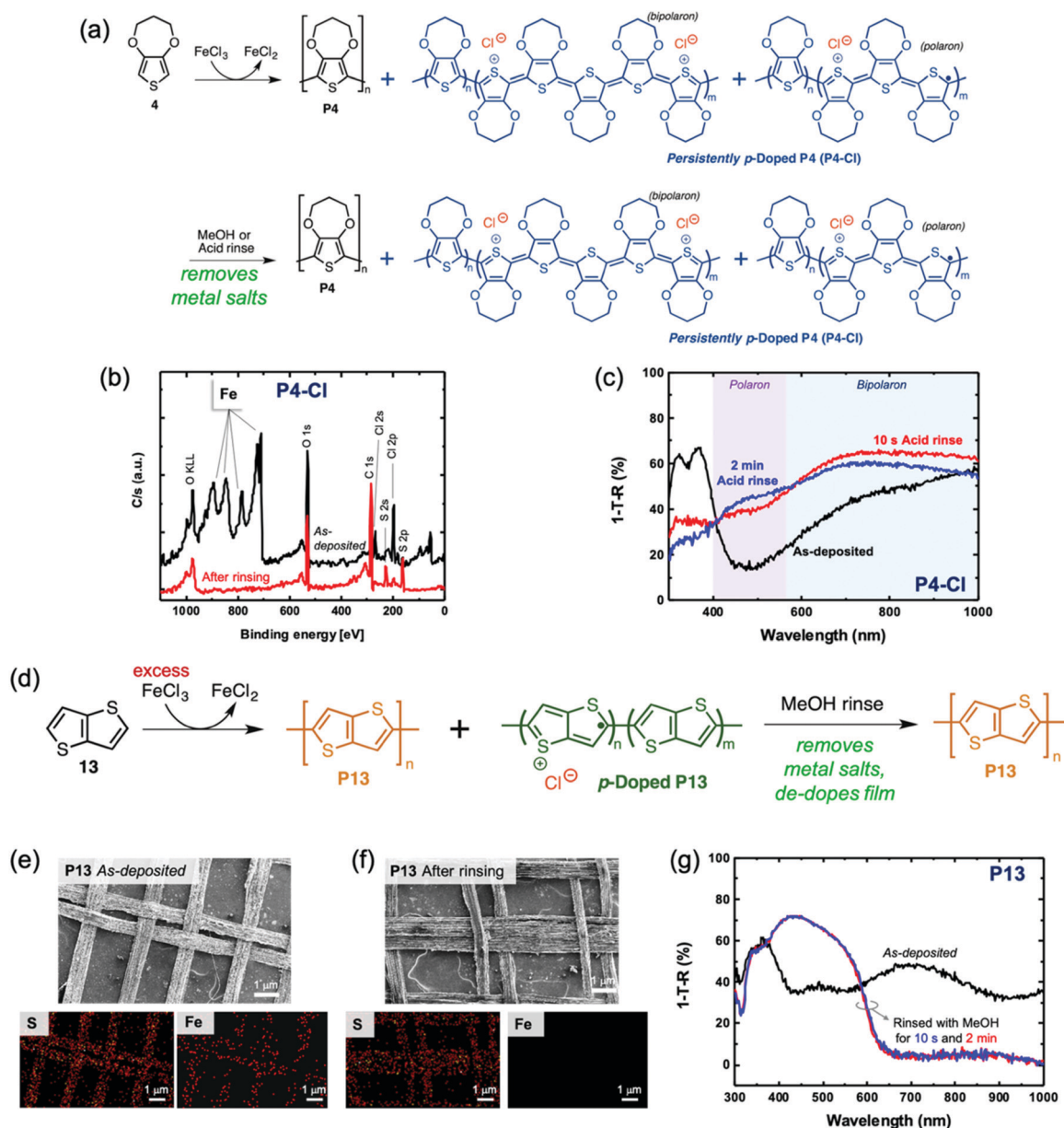
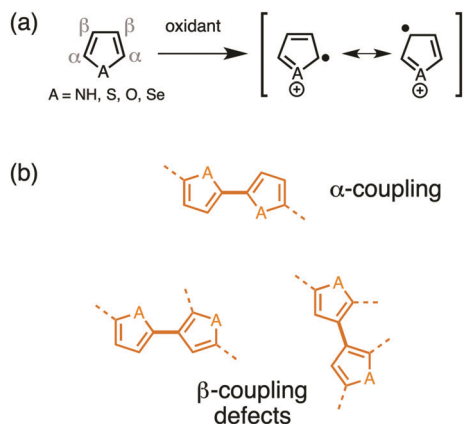


Fig. 3 (a) Reaction scheme illustrating the persistent p-doping of **P4-Cl** subsequent to methanol or acid rinsing. (b) X-ray photoelectron spectra of **P4-Cl** thin films before and after rinsing with 0.5 M HCl. Adapted with permission from ref. 74. (c) UV-vis 1-transmission-reflectance (1-T-R) spectra of an as-deposited **P4-Cl** film and the same film after rinsing with a 0.5 M HCl solution. Adapted with permission from ref. 74. (d) Reaction scheme illustrating the dedoping of **P13** subsequent to methanol rinsing. SEMs and corresponding EDX spectra (S and Fe atoms) of **P13** films on banana fiber fabric (e) before and (f) after rinsing with methanol. (g) UV-vis 1-T-R of an as-deposited **P13** film and the same film after a 2 minute methanol rinse. Adapted with permission from ref. 74.

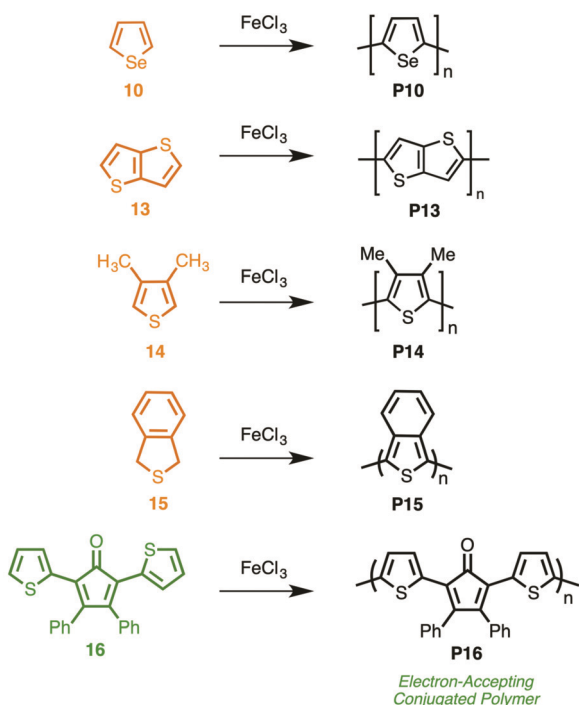
component electrodes in various solid-state pseudocapacitive devices, with effective operating windows of approximately 1.2 V.<sup>82</sup> When a thick film of **P14** is used as one of two electrodes in an unsymmetric solid state device, the operating window was found to increase to 1.5 V, with minimal changes to the observed charge and ion transport impedances displayed by **P2-Cl**.

Finally, work has been done by Gleason *et al.* concerning **P15**.<sup>96</sup> Originally synthesized by Wudl *et al.*, **P15** has a very low band gap of 1 eV.<sup>97</sup> Using oCVD, the synthesis of **P15** was performed in one step between  $\text{FeCl}_3$  oxidant and monomer **15**.

Successful dedoping of the films was confirmed *via* X-ray photoelectron and ultra-violet visible spectroscopy. By heating the substrate stage to higher temperatures, larger conjugation lengths were obtained in films of **P15**. This translated to tunable band gaps spanning from 1.14 to 1.05 eV, relatively consistent with reports of solution synthesized **P15**. Interestingly, two discrete chemical reactions are needed to transform monomer **15** into **P15** using traditional, solution-phase organic synthesis.<sup>98,99</sup> In contrast, this complex transformation is readily achieved in one step during reactive vapor deposition. This observation highlights



**Scheme 4** (a) Important resonance structures of the radical cation formed during oxidative polymerization. (b) The different monomer coupling arrangements that can occur in resulting polymers.



**Scheme 5** Reactive vapor deposition of polymers with notable optical or electronic properties.

the unique synthetic advantages of reactive vapor deposition: an absence of solvation effects and the availability of *in situ* heating can potentially drive difficult chemical transformations to completion.

Until very recently, all of the polymer films created using reactive vapor deposition have been exclusively hole transporting materials with high-lying valence band edges. Because an oxidative polymerization underpins all of the polymer deposition protocols discussed herein, a limited electronic variation is to be expected. As shown in Scheme 6, electron donating groups in the  $\beta$ -positions of the thiophene ring will stabilize the radical cation intermediate, thus decreasing the activation energy required to form this reactive

intermediate and increasing the reaction rate for this step. Electron rich parent heterocycles lacking  $\beta$ -substituents, such as pyrrole, thiophene and selenophene, also natively stabilize radical cations. In contrast, electron withdrawing substituents will destabilize a radical cation, which will increase the activation barrier to access this necessary reactive intermediate and decrease the overall rate of polymerization. Inconveniently, the same electron withdrawing substituents are necessary for accessing electron-conducting materials with low-lying conduction band edges.<sup>100</sup> Therefore, n-type polymers are challenging to synthesize *via* an oxidative polymerization reaction.

Andrew *et al.* provided a possible solution to this issue by using a donor-acceptor-donor triad, **16**,<sup>101</sup> with a large dihedral angle between the donor and acceptor moieties, which effectively electronically decoupled the two components<sup>102</sup> and allowed the electron-rich donor to participate in an oxidative polymerization reaction. Monomer **16** contains electron-rich thiophene substituents in the 2,5-positions of an electron-accepting cyclopentadienone (CPD) ring. Fig. 6a illustrates how the CPD moiety transforms from an unstable antiaromatic system to a stable dianion upon two-electron reduction, rendering it a strong electron acceptor. Similar n-dopable analogues were reported by Wudl *et al.*<sup>67</sup> In the case of monomer **16**, the thiophene rings (donors) are twisted out of conjugation with the cyclopentadienone moiety (acceptor), allowing them to be oxidized by iron(III) chloride despite the presence of an electron withdrawing group. Given the high molar mass of **16**, films of **P16** were fabricated *via* an oCVD protocol using Chamber 2. Ultra-violet photoelectron spectroscopy (UPS) revealed an especially deep-lying valence band edge at  $-6.7 \pm 0.2$  eV (as determined from three separate sample measurements). The optical band gap of **P16** was calculated as 1.50 eV *via* UV-vis spectroscopy (using the absorption onset of the lowest-energy  $n-\pi^*$  transition). Fig. 6b compares the electronic band structure of **P16** to those of the electron transporter  $C_{60}$  and a representative vapor deposited p-type polymer.

## Future directions

Whereas the engineering applications of reactive vapor deposition are currently explored across multiple research groups, comparatively fewer efforts are dedicated to expanding the scope of polymer structures that can be accessed. As stated earlier, reactive vapor deposition can be perceived as a nascent, solvent-free synthetic technique with which to access a plethora of conjugated oligomers and polymers. Since solubilizing side chains are not required to synthesize and deposit polymer films, fewer synthetic steps are required to access appropriate monomers for RVD as compared to conventional solution polymerization reactions, thus improving the synthetic accessibility<sup>103</sup> and, therefore, cost of vapor deposited polymers. RVD is also a pragmatic polymerization approach for monomers with limited solubility, which may have otherwise been abandoned by synthetic materials chemists utilizing conventional polymerization reactions, such as Suzuki, Stille and Grignard metathesis polymerization reactions. For example, the cyclopentadienone-containing monomer **16** was

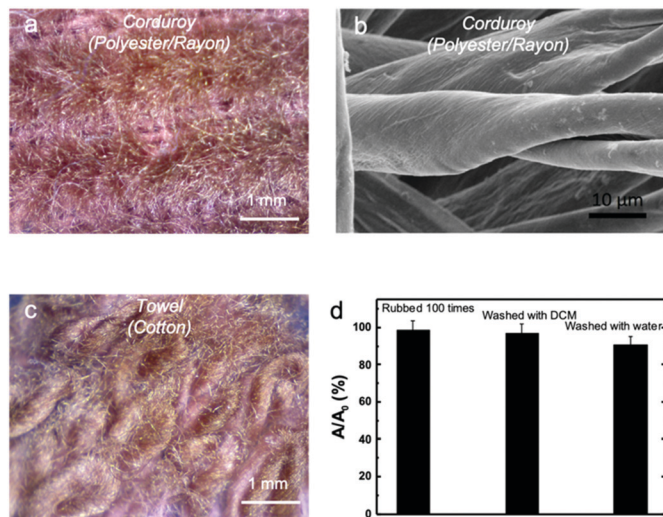


Fig. 4 (a) Optical micrograph and (b) SEM of a corduroy fabric vapor coated with **P13** in Chamber 2 (after rinsing). (c) Optical micrograph of a cotton towel vapor coated with **P13** in Chamber 2 (after rinsing). (d) Percent change in surface color of a **P13**-coated cotton towel after rubbing and solvent washing. Adapted with permission from ref. 74.

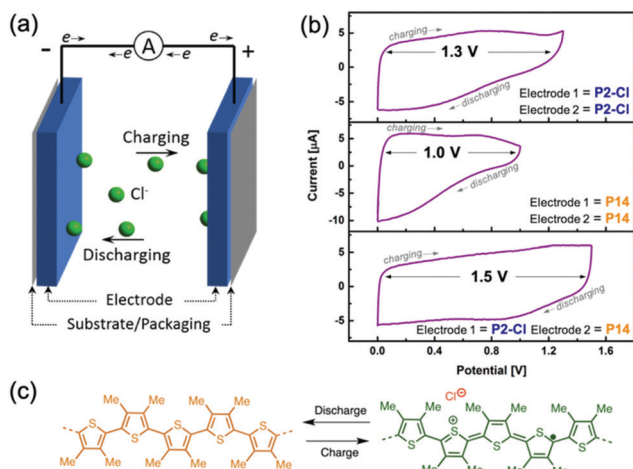
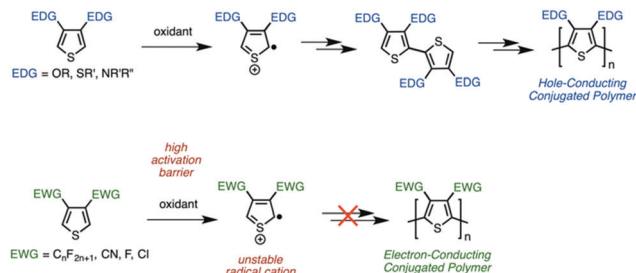


Fig. 5 (a) Schematic of charge–discharge cycling in a two-electrode supercapacitor. (b) Two-electrode cyclic voltammograms recorded in 0.5 M H<sub>2</sub>SO<sub>4</sub> during one charging and discharging cycle for (top) two 10 μm-thick **P2-Cl** electrodes on polyimide, (middle) two 10 μm-thick **P14** electrodes on polyimide, and (bottom) an asymmetric supercapacitor comprised of one 10 μm-thick **P2-Cl** electrode and one 10 μm-thick **P14** electrode on polyimide. The asymmetric device displays an expanded voltage window as compared to the symmetric devices. (c) Chemical changes accompanying charge–discharge cycling.

originally reported by Wudl *et al.* in 2008,<sup>67</sup> but was abandoned from subsequent lines of investigation as the resulting polymers could not be solution processed to perform necessary characterizations and fabricate devices (Fig. 7). In stark contrast, monomer **16** readily afforded uniform polymer films on textile substrates upon being subjected to RVD.<sup>101</sup> Therefore, we believe that RVD merits increased attention from the synthetic community. In this section, we highlight known structural deficiencies in vapor deposited polymers and selected synthetic challenges that warrant improvements in the near term.



Scheme 6 Comparison between the effects of electron-donating (top) versus electron-accepting (bottom) substituents on the oxidative polymerization of heterocyclic monomers.

To date, reactive vapor deposition recipes that afford regio-regular polymers are unknown. All known protocols use an oxidative polymerization reaction to create conjugated polymer films, which proceeds *via* coupling of charged radical intermediates. In the absence of directing groups or other, deliberately introduced stereoelectronic effects, radical coupling proceeds in a statistical fashion that leads to regiorandom polymers when unsymmetric monomers are used (Fig. 8). Indeed, historically, the solution-phase oxidative polymerization of 3-substituted thiophene derivatives has always been used to synthesize regiorandom poly(3-alkylthiophene) polymers.<sup>104</sup> Regioregularity is an important and desirable feature, especially in poly(3-alkylthiophene)s, in which regioregularity enables lamellar packing structures that lead to optimized charge carrier mobilities.<sup>105</sup> In contrast, an absence of regioregularity results in low charge carrier mobilities. Furthermore, the presence of β-coupling defects should further inhibit long-range order and, consequentially, charge carrier mobility. To wit, the best known hole mobility for regioregular poly(3-hexylthiophene) synthesized *via* a Grignard metathesis polymerization reaction is 1.37 cm<sup>2</sup> V<sup>-1</sup> s<sup>-1</sup>,<sup>106</sup> whereas the average hole mobility of vapor deposited poly(thiophene) pales in comparison, at 3.74 × 10<sup>-3</sup> cm<sup>2</sup> V<sup>-1</sup> s<sup>-1</sup>.<sup>87</sup> Process, surface,

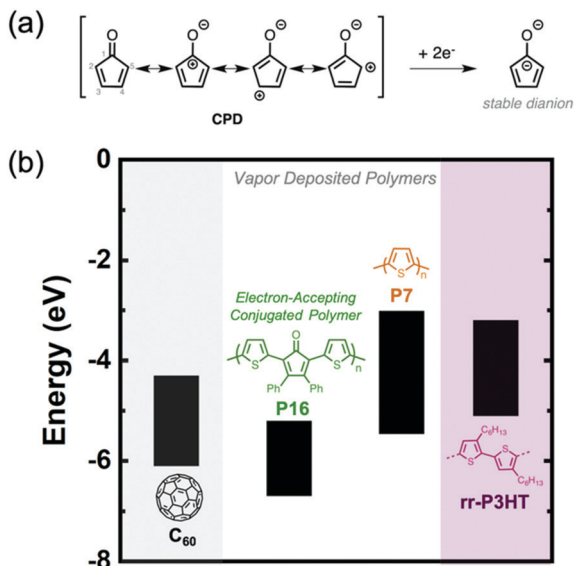


Fig. 6 (a) The cyclopentadienone acceptor moiety. (b) Comparison between the electronic band structures of **P16** with canonical hole and electron transporters.

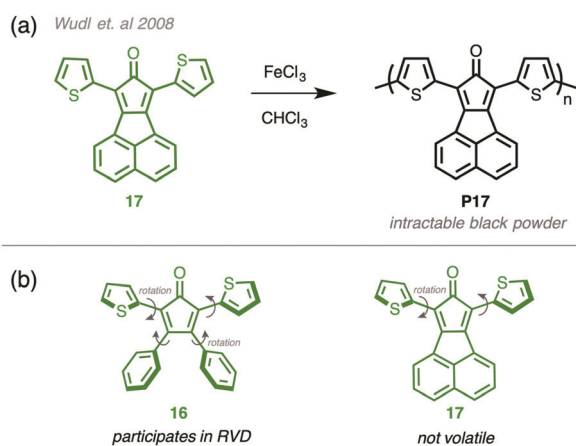


Fig. 7 (a) Solution-phase oxidative polymerization of monomer **17** yields an insoluble polymer **P17**. (b) Substituents with many rotational degrees of freedom impart sufficient volatility, which is needed for RVD, but inhibit  $\pi$ -stacking that enables efficient charge transport.

and/or reaction modifications that allow access to vapor deposited, regioregular polymers will be impactful for the fabrication of flexible transistor arrays. The concentration of  $\beta$ -defects in vapor deposited polymer films can potentially be addressed by taking cues from the direct arylation polymerization community,<sup>107</sup> which has been investigating various strategies to favor  $\alpha$ -coupling events over  $\beta$ -coupling side reactions. Additionally, one could vary the counterion of the metal oxidant used for RVD such that tight ion pairing between the thiophene radical cation intermediate and the counterion is introduced, which should bias the formation of one kind of linkage ( $\alpha$ - or  $\beta$ -) over the other, depending on the polarizability and steric bulk of the counterion.

While a few vapor deposited copolymers are reported to date, the polymer films created from multiple monomers do

not possess the same level of sequence regularity and control as solution-synthesized counterparts. Sequence control is important for accessing semiconducting polymers with tunable band gaps.<sup>108</sup> Donor-acceptor conjugated polymers synthesized using conventional solution polymerization reliably contain alternating electron-rich and electron-poor moieties in the polymer backbone, which results in the observation of a characteristic charge-transfer band in their UV-vis-NIR absorption spectra. The absorption maximum and oscillator strength of this charge transfer band can be tailored by judiciously choosing the electron-rich and electron-poor moieties contained in the polymer repeat unit. Analogous band-gap tuning in reactive vapor deposited polymers has not been demonstrated to date, since most known iterations of vapor deposited semiconductors are predominantly thiophene-based. A limited scope of accessible repeat unit structures means that the strength of donor-acceptor interactions and, transitively, the absorption maximum of donor-acceptor polymers cannot be tuned.

Moreover, all thiophene-based semiconductors are primarily hole conductors (p-type) with approximately similar band gaps (ca. 2.2–2.4 eV) and valence band edges ( $5.2 \pm 0.2$  eV), meaning that systematically engineering Type II heterojunctions for organic solar cells and light emitting diodes<sup>109</sup> is challenging. Therefore, efforts to develop vapor deposition recipes for new p-type and n-type monomers, including sulfur-free compounds, are warranted. Particularly for wearable and implantable electronics, a transition away from aniline and thiophene-based polymers is essential because of recent, troubling reports of acute liver toxicity in drugs containing these moieties.<sup>110,111</sup>

As previously discussed, the singular reaction underpinning all known vapor deposition recipes is the oxidative polymerization reaction. This narrow reaction scope means that only electron-rich monomers will practically afford polymer films (Scheme 6) and, correspondingly, any resulting polymer films will have high-lying valence band edges that will only be suitable for hole conduction/injection/extraction.<sup>100</sup> Although Andrew *et al.* reported a strategy to circumvent this limitation—use of a donor-acceptor-donor triad in which the donors are twisted out of conjugation with acceptor<sup>101</sup>—the monomer used in that study contained many rotational degrees of freedom (Fig. 7), which typically inhibit  $\pi$ -stacking in the condensed phase. Consequently, films of **P16** were expected to display low charge carrier mobilities. Unfortunately, Andrew *et al.* also found that substituents with higher degrees of rotational freedom were necessary to volatilize monomers at reasonable temperatures and obtain polymer films using Chamber 2. For example, the comparatively planar monomer **17**, which should generate crystalline polymer films, did not yield a practical vapor plume when heated to within 25 °C of its observed decomposition temperature at a chamber pressure of 100 mTorr. Therefore, more creative strategies are needed to vapor deposit n-type polymers with optimized optical and electronic properties. Impactful advances will likely be made by adapting other unexplored, bicomponent reactions<sup>112</sup> to RVD protocols, thus allowing access to a broader array of precursors with desirable structural and electronic variations.

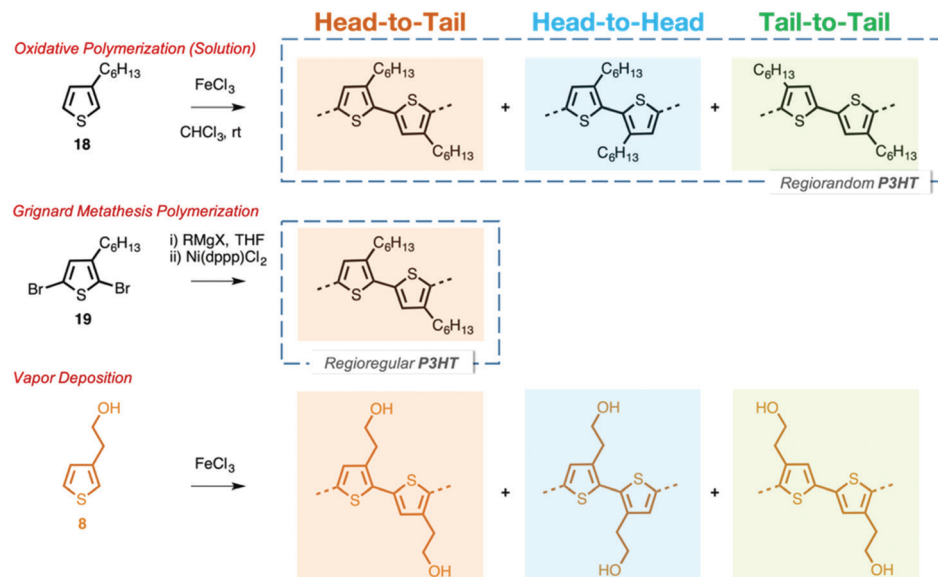


Fig. 8 Comparison of regioregularity in reaction products produced through different polymerization methods.

## Conflicts of interest

There authors declare no conflicts.

## Acknowledgements

This material is based upon work supported by the National Science Foundation under CHEM MSN 1807743. T. L. A. also gratefully acknowledges support from the David and Lucile Packard Foundation.

## References

- L. Dou, Y. Liu, Z. Hong, G. Li and Y. Yang, *Chem. Rev.*, 2015, **115**, 12633–12665.
- P. M. Beaujuge and J. R. Reynolds, *Chem. Rev.*, 2010, **110**, 268–320.
- X. Guo, A. Facchetti and T. J. Marks, *Chem. Rev.*, 2014, **114**, 8943–9021.
- D. Choi, M. Chang and E. Reichmanis, *Adv. Funct. Mater.*, 2015, **25**, 920–927.
- C. R. McNeill, *Energy Environ. Sci.*, 2012, **5**, 5653–5667.
- T. P. Martin, A. J. Wise, E. Busby, J. Gao, J. D. Roehling, M. J. Ford, D. S. Larsen, A. J. Moule and J. K. Grey, *J. Phys. Chem. B*, 2013, **117**, 4478–4487.
- Y. Gao, T. P. Martin, E. T. Niles, A. J. Wise, A. K. Thomas and J. K. Grey, *J. Phys. Chem. C*, 2010, **114**, 15121–15128.
- S. Savagatrup, A. D. Printz, T. F. O'Connor, A. V. Zaretski and D. J. Lipomi, *Chem. Mater.*, 2014, **26**, 3028–3041.
- M. Kaltenbrunner, T. Sekitani, J. Reeder, T. Yokota, K. Kuribara, T. Tokuhara, M. Drack, R. Schwodiauer, I. Graz, S. Bauer-Gogonea, S. Bauer and T. Someya, *Nature*, 2013, **499**, 458–463.
- O. Awartani, B. I. Lemanski, H. W. Ro, L. J. Richter, D. M. DeLongchamp and B. T. O'Connor, *Adv. Energy Mater.*, 2013, **3**, 399–406.
- G. Schwartz, B. C.-K. Tee, J. Mei, A. L. Appleton, D. H. Kim, H. Wang and Z. Bao, *Nat. Commun.*, 2013, **4**, 1859.
- M. C. Barr, J. A. Rowehl, R. P. Lunt, J. Xu, A. Wang, C. M. Boyce, S. G. Im, V. Bulovic and K. K. Gleason, *Adv. Mater.*, 2011, **23**, 3500–3505.
- L. Allison, S. Hoxie and T. L. Andrew, *Chem. Commun.*, 2017, **53**, 7182–7193.
- T. L. Andrew, L. Zhang, N. Cheng, M. Baima, J. J. Kim, L. Allison and S. Hoxie, *Acc. Chem. Res.*, 2018, **51**, 850–859.
- M. E. Alf, A. Asatekin, M. C. Barr, S. H. Baxamusa, H. Chelawat, G. Ozaydin-Ince, C. D. Petruczok, R. Sreenivasan, W. E. Tenhaeff, N. J. Trujillo, S. Vaddiraju, J. Xu and K. K. Gleason, *Adv. Mater.*, 2010, **22**, 1993–2027.
- S. H. Baxamusa, S. G. Im and K. K. Gleason, *Phys. Chem. Chem. Phys.*, 2009, **11**, 5227–5240.
- J. M. D'Arcy, H. D. Tran, V. C. Tung, A. K. Tucker-Schwartz, R. P. Wong, Y. Yang and R. B. Kaner, *Proc. Natl. Acad. Sci. U. S. A.*, 2010, **107**, 19673–19678.
- M. H. Gharahcheshmeh and K. K. Gleason, *Adv. Mater. Interfaces*, 2019, **6**, 1801564.
- P. Kovacik, G. del Hierro, W. Livernois and K. K. Gleason, *Mater. Horiz.*, 2015, **2**, 221–227.
- R. A. Ruehrwein, *US Pat.*, 3364084, 1968.
- A. G. Thompson, *Mater. Lett.*, 1997, **30**, 255–263.
- H. M. Manasevit, *Appl. Phys. Lett.*, 1968, **156**, 10–14.
- 50 Years Progress in Crystal Growth*, ed. R. Feigelson, Elsevier Science, Amsterdam, 2004.
- P. D. Dapkus, *Annu. Rev. Mater. Sci.*, 1982, **12**, 243–269.
- M. Meyyappan, *J. Phys. D: Appl. Phys.*, 2009, **42**, 15.
- B. T. Williams and M. W. Hayes, *Nature*, 1966, **209**, 769–773.
- H. Biederman, *Surf. Coat. Technol.*, 2000, **125**, 371–376.

- 28 K. K. S. Lau, J. Bico, K. B. K. Teo, M. Chhowalla, G. A. J. Amaratunga, W. I. Milne, G. H. McKinley and K. K. Gleason, *Nano Lett.*, 2003, **3**, 1701–1705.
- 29 R. Muñoz and C. Gómez-Aleixandre, *Chem. Vap. Deposition*, 2013, **19**, 297–322.
- 30 T. Suntola and J. Antson, *US Pat.*, 4058430, 1977.
- 31 S. M. George, *Chem. Rev.*, 2010, **110**, 111–131.
- 32 R. W. Johnson, A. Hultqvist and S. F. Bent, *Biochem. Pharmacol.*, 2014, **17**, 236–246.
- 33 B. M. Knez, K. Nielsch and L. Niinisto, *Adv. Mater.*, 2007, **19**, 3425–3438.
- 34 D. Muñoz-Rojas, V. H. Nguyen, C. Masse, D. Huerta, S. Aghazadehchors, C. Jiménez and D. Bellet, *C. R. Phys.*, 2017, **18**, 391–400.
- 35 P. Poodt, V. Tiba, F. Werner, J. Schmidt, A. Vermeer and F. Roozeboom, *J. Electrochem. Soc.*, 2011, **158**, 937–940.
- 36 Diamond-MT, <https://www.diamond-mt.com/>, (accessed March 2019).
- 37 K. M. Vaeth and K. F. Jensen, *Adv. Mater.*, 1999, **11**, 814–820.
- 38 Y. Mao and K. K. Gleason, *Langmuir*, 2004, **20**, 2484–2488.
- 39 K. Chan and K. K. Gleason, *Langmuir*, 2005, **21**, 8930–8939.
- 40 M. Gupta, V. Kapur, N. M. Pinkerton and K. K. Gleason, *Chem. Mater.*, 2008, **20**, 1646–1651.
- 41 L. C. Bradley and M. Gupta, *Langmuir*, 2015, **31**, 7999–8005.
- 42 K. C. K. Cheng, M. A. Bedolla-Pantoja, Y. Kim, J. V. Gregory, F. Xie, A. de France, C. Hussal, K. Sun, N. L. Abbot and J. Lahan, *Science*, 2018, **362**, 804–808.
- 43 S. J. Yu, K. Pak, M. J. Kwak, M. Joo, B. J. Kim, M. S. Oh, J. Baek, H. Park, G. Choi, D. H. Kim, J. Choi, Y. Choi, J. Shin, H. Moon, E. Lee and S. G. Im, *Adv. Eng. Mater.*, 2017, **20**, 1700622.
- 44 A. Asatekin, M. C. Barr, S. H. Baxamusa, K. K. S. Lau, W. Tenhaeff, J. Xu and K. K. Gleason, *Mater. Today*, 2010, **13**, 26–33.
- 45 W. E. Tenhaeff and K. K. Gleason, *Adv. Funct. Mater.*, 2008, **18**, 979–992.
- 46 E. G. Linder and A. P. Davis, *J. Phys. Chem.*, 1931, **35**, 3649–3672.
- 47 R. K. Sadhir and K. F. Schoch, *Thin Solid Films*, 1993, **223**, 154–160.
- 48 L. M. H. Groenewoud, A. E. Weinbeck, G. H. M. Engbers and J. Feijen, *Synth. Met.*, 2002, **126**, 143–149.
- 49 M. Meyyappan, *J. Phys. D: Appl. Phys.*, 2011, **44**, 174002.
- 50 B. R. Sreenivasan and K. K. Gleason, *Chem. Vap. Deposition*, 2009, **15**, 77–90.
- 51 R. B. Bjorklund, *J. Chem. Soc.*, 1987, **83**, 1507–1514.
- 52 M. Mueller, M. Fabretto, D. Evans, P. Hojati-Talemi, C. Gruber and P. Murphy, *Polymer*, 2012, **53**, 2146–2151.
- 53 R. Brooke, P. Cottis, P. Talemi, M. Fabretto, P. Murphy and D. Evans, *Prog. Mater. Sci.*, 2017, **86**, 127–146.
- 54 Y. Wang, G. A. Sotzing and R. A. Weiss, *Chem. Mater.*, 2008, **20**, 2574–2582.
- 55 S. L. Shenoy, D. Cohen, C. Erkey and R. A. Weiss, *Ind. Eng. Chem. Res.*, 2002, **41**, 1484–1488.
- 56 T. Ojio and S. Miyata, *Polym. J.*, 1986, **18**, 95–98.
- 57 J. M. D'Arcy, M. F. El-Kady, P. P. Khine, L. Zhang, S. H. Lee, N. R. Davis, D. S. Liu, M. T. Yeung, S. Y. Kim, C. L. Turner, A. T. Lech, P. T. Hammond and R. B. Kaner, *ACS Nano*, 2014, **8**, 1500–1510.
- 58 B. Winther-Jensen, J. Chen, K. West and G. Wallace, *Macromolecules*, 2004, **37**, 5930–5935.
- 59 H. Wang, Y. Diao, M. Rubin, L. M. Santino, Y. Lu and J. M. Darcy, *ACS Appl. Nano Mater.*, 2018, **1**, 1219–1227.
- 60 M. A. Ali, H. Kim, K. Jeong, H. Soh and J. Lee, *Electron. Mater. Lett.*, 2010, **6**, 17–22.
- 61 M. A. Ali, K. Wu, J. McEwan and J. Lee, *Synth. Met.*, 2018, **244**, 113–119.
- 62 A. Mohammadi, M. A. Hasan, B. Liedberg, I. Lundstrom and W. R. Salaneck, *Synth. Met.*, 1986, **14**, 189–197.
- 63 L. Zhang, M. Fairbanks and T. L. Andrew, *Adv. Funct. Mater.*, 2017, **27**, 1700415.
- 64 D. C. Trivedi, *Bull. Mater. Sci.*, 1999, **22**, 447–455.
- 65 A. A. Rakic, S. Trifunovic and G. Ciric-Marjanovic, *Synth. Met.*, 2014, **192**, 56–65.
- 66 D. Bhattacharyya, R. M. Howden, D. C. Borrelli and K. K. Gleason, *J. Polym. Sci., Part B: Polym. Phys.*, 2012, **50**, 1329–1351.
- 67 W. Walker, B. Veldman, R. Chiechi, S. Patil, M. Bendikov and F. Wudl, *Macromolecules*, 2008, **41**, 7278–7280.
- 68 S. R. Forrest, *Chem. Rev.*, 1997, **97**, 1793–1896.
- 69 Angstrom Engineering, <https://angstromengineering.com/>, accessed March 2019.
- 70 A. M. Coclite, R. M. Howden, D. C. Borrelli, C. D. Petruczuk, R. Yang, J. L. Yague, A. Ugur, N. Chen, S. Lee, W. J. Jo, A. Liu, X. Wang and K. K. Gleason, *Adv. Mater.*, 2013, **25**, 5392–5423.
- 71 G. Bengasi, K. Baba, G. Frache, J. Desport, P. Gratia, K. Heinze and N. D. Boscher, *Angew. Chem., Int. Ed.*, 2019, **58**, 2103–2108.
- 72 K. Baba, G. Bengasi, D. El Assad, P. Grysan, E. Lentzen, K. Heinze, G. Frache and N. D. Boscher, *Eur. J. Org. Chem.*, 2019, DOI: 10.1002/ejoc.201900045.
- 73 T. Yoshimura, S. Tatsuuru and W. Sotoyama, *Appl. Phys. Lett.*, 1991, **59**, 482–484.
- 74 N. Cheng, L. Zhang, J. J. Kim and T. L. Andrew, *J. Mater. Chem. C*, 2017, **5**, 5787–5796.
- 75 L. Zhang and T. L. Andrew, *Adv. Mater. Interfaces*, 2017, **4**, 1700873.
- 76 S. E. Atanasov, M. D. Losego, F. Gong, E. Sacht, J. P. Maria, P. S. Williams and G. N. Parsons, *Chem. Mater.*, 2014, **26**, 3471–3478.
- 77 X. Wang, X. Zhang, L. Sun, D. Lee, S. Lee, M. Wang, J. Zhao, Y. Shao-Horn, M. Dinca, T. Palacios and K. K. Gleason, *Sci. Adv.*, 2018, **4**, eaat5780.
- 78 J. P. Lock, S. G. Im and K. K. Gleason, *Macromolecules*, 2006, **39**, 5326–5329.
- 79 S. G. Im, D. Kusters, W. Choi, S. H. Baxamusa, M. C. M. van de Sanden and K. K. Gleason, *ACS Nano*, 2008, **2**, 1959–2008.
- 80 S. Kaviani, M. M. Ghaleni, E. Tavakoli and S. Nejati, *ACS Appl. Polym. Mater.*, 2019, **1**, 552–560.
- 81 L. Zhang, W. Viola and T. L. Andrew, *ACS Appl. Mater. Interfaces*, 2018, **10**, 36834–36840.
- 82 L. Zhang and T. L. Andrew, *ACS Appl. Mater. Interfaces*, 2018, **10**, 38574–38580.

- 83 Y. Y. Smolin, M. Soroush and K. S. Lau, *Ind. Eng. Chem. Res.*, 2017, **56**, 6221–6228.
- 84 L. Zhang, M. Baima and T. L. Andrew, *ACS Appl. Mater. Interfaces*, 2017, **9**, 32299–32307.
- 85 L. K. Allison and T. L. Andrew, *Adv. Mater. Technol.*, 2019, **4**, 1800615.
- 86 J. J. Kim, L. K. Allison and T. L. Andrew, *Sci. Adv.*, 2019, **5**, eaaw0463.
- 87 D. C. Borrelli, S. Lee and K. K. Gleason, *J. Mater. Chem. C*, 2014, **2**, 7223–7231.
- 88 D. C. Borrelli, M. C. Barr, V. Bulovic and K. K. Gleason, *Sol. Energy Mater. Sol. Cells*, 2012, **99**, 190–196.
- 89 L. L. Miller and K. R. Mann, *Acc. Chem. Res.*, 1996, **29**, 417–423.
- 90 R. Rathore, A. S. Kumar, S. V. Lindeman and J. K. Kochi, *J. Org. Chem.*, 1998, **63**, 5847–5856.
- 91 H. Goktas, X. Wang, N. D. Boscher, S. Torosian and K. K. Gleason, *J. Mater. Chem. C*, 2016, **4**, 3403–3414.
- 92 D. Bhattacharyya, K. Senecal, P. Marek, A. Senecal and K. K. Gleason, *Adv. Funct. Mater.*, 2011, **21**, 4328–4337.
- 93 S. Vaddiraju, K. Seneca and K. K. Gleason, *Adv. Funct. Mater.*, 2008, **18**, 1929–1938.
- 94 S. Vaddiraju and K. K. Gleason, *Nanotechnology*, 2010, **21**, 125503.
- 95 D. Bhattacharyya and K. K. Gleason, *J. Mater. Chem.*, 2012, **22**, 405–410.
- 96 D. C. Borrelli and K. K. Gleason, *Macromolecules*, 2013, **46**, 6169–6176.
- 97 F. Wudl, M. Kobayashi and A. J. Heeger, *J. Org. Chem.*, 1984, **49**, 3382–3384.
- 98 K. Kawabata and H. Goto, *J. Mater. Chem.*, 2012, **22**, 23514–23524.
- 99 W. Chen, G. A. Bowmaker, J. M. Seakins and R. P. Cooney, *Synth. Met.*, 2002, **128**, 215–230.
- 100 C. R. Newman, C. D. Frisbie, D. A. da Silva Filho, J.-L. Brédas, P. C. Ewbank and K. R. Mann, *Chem. Mater.*, 2004, **16**, 4436–4451.
- 101 D. Bilger, K. Park and T. L. Andrew, *Synth. Met.*, 2019, **250**, 1–6.
- 102 J. L. Brédas, G. B. Street, B. Themans and J. M. Andre, *J. Chem. Phys.*, 1985, 1323–1329.
- 103 T. P. Osedach, T. L. Andrew and V. Bulović, *Energy Environ. Sci.*, 2013, **6**, 711–718.
- 104 J. M. Lobe, T. L. Andrew, V. Bulović and T. M. Swager, *ACS Nano*, 2012, **6**, 3044–3056.
- 105 I. Osaka and R. D. McCullough, *Acc. Chem. Res.*, 2008, **41**, 1202–1214.
- 106 H. C. Avila, P. Serrano, A. R. J. Barreto, Z. Ahmed, C. D. P. Gouvêa, C. Vilani, R. B. Capaz, C. F. N. Marchiori and M. Cremona, *Org. Electron.*, 2018, **58**, 33–37.
- 107 N. S. Gobalasingham and B. C. Thompson, *Prog. Polym. Sci.*, 2018, **83**, 135–201.
- 108 Y. Li, *Acc. Chem. Res.*, 2012, **45**, 723–733.
- 109 T. M. Clarke and J. R. Durrant, *Chem. Rev.*, 2010, **110**, 6736–6767.
- 110 C. K. Jaladanki, N. Taxak, R. A. Varikoti and P. V. Bharatam, *Chem. Res. Toxicol.*, 2015, **28**, 2364–2376.
- 111 E. Raschi and F. de Ponti, *World J. Hepatol.*, 2017, **9**, 30–37.
- 112 L. Kurti and B. Czako, *Strategic Applications of Named Reactions in Organic Synthesis*, Elsevier Academic Press, Burlington, 2005.